

Topology-optimized Dual-Polarization Dirac Cones

Zin Lin^{1,*}, Lysander Christakis^{2,*}, Yang Li^{1,*}, Eric Mazur¹, Alejandro W. Rodriguez³, and Marko Lončar^{1†}

¹John A. Paulson School of Engineering and Applied Sciences, Harvard University, Cambridge, MA 02138

²Department of Physics, Yale University, New Haven, CT 06511 and

³Department of Electrical Engineering, Princeton University, Princeton, NJ, 08544

(Dated: September 22, 2017)

We apply a large-scale computational technique, known as topology optimization, to the inverse design of photonic Dirac cones. In particular, we report on a variety of photonic crystal geometries, realizable in simple isotropic dielectric materials, which exhibit dual-polarization Dirac cones. We present photonic crystals of different symmetry types, such as four-fold and six-fold rotational symmetries, with Dirac cones at different points within the Brillouin zone. The demonstrated and related optimization techniques open new avenues to band-structure engineering and manipulating the propagation of light in periodic media, with possible applications to exotic optical phenomena such as effective zero-index media and topological photonics.

PACS numbers: 42.70.Qs, 78.67.Pt, 02.30.Zz, 02.60.Pn

Dirac cones (DC), or conical dispersions, have received broad attention due to their special properties affecting light transport in photonic systems, such as effective zero-index behavior [1–7], exceptional points [8, 9], photonic *Zitterbewegung* [10], and topologically protected states [11, 12]. So far, DCs have been primarily studied in simple geometries based on circular pillars or air holes on a periodic lattice [1–3, 5, 7, 13]. One exception is our previous work [9], which exploited topology optimization (TO) techniques to demonstrate higher-order DCs (precursors to exceptional points [8, 9]) in complex structures. TO, which was first proposed more than a decade ago [14], employs gradient-based algorithms to efficiently handle a very large design space, considering every pixel or voxel as a degree of freedom (DOF) in an extensive 2D or 3D computational domain [15]. Recently, inverse-designed materials based on TO have been utilized to improve the performance of optical devices such as mode splitters, demultiplexers, and wavelength converters [15–20]. Here, we apply TO toward the design of unprecedented dispersion features in photonic crystals (PhC), namely, two overlapping DCs with dual polarizations (DPDC): one having transverse magnetic polarization ($\mathbf{H} \cdot \hat{\mathbf{z}} = 0$) and the other having transverse electric polarization ($\mathbf{E} \cdot \hat{\mathbf{z}} = 0$). We show that if designed at the Γ point of the Brillouin zone, such PhCs exhibit effective zero-index behavior. Furthermore, we demonstrate DPDCs at the \mathbf{K} point of a hexagonal PhC, which has implications for all-dielectric topological photonics [12, 21].

Recent years have witnessed an exciting quest for exotic composite materials along with unusual states of matter involving enhanced optical, mechanical, and quantum properties [22–25]. However, there has been comparatively less effort devoted to discovering unconventional structures that can enhance the functionality of ordinary materials, such as ubiquitous low-loss isotropic dielectrics. Our work represents an effort to leverage the capabilities of established but underutilized inverse design tools to uncover increased functionalities for simple dielectrics.

Dual-polarization Dirac Cones.—Power emitted by a time-harmonic current source $\mathbf{J} \sim e^{i\omega t}$, proportional to the lo-

cal density of states (LDOS), offers a convenient optimization framework for designing eigenmodes at a given frequency ω . This follows the well-known principle that emitted power, $f(\mathbf{E}, \mathbf{J}, \omega; \epsilon) = -\text{Re} \left[\int \mathbf{J}^* \cdot \mathbf{E} \, d\mathbf{r} \right]$, is maximized when the source couples to a long-lived resonance [26]. Here, the electric field \mathbf{E} is simply the solution of the steady-state Maxwell equation, $\nabla \times \frac{1}{\mu} \nabla \times \mathbf{E} - \omega^2 \epsilon(\mathbf{r}) \mathbf{E} = i\omega \mathbf{J}$. The goal of TO is to discover the dielectric profile $\epsilon(\mathbf{r})$ that maximizes f for any given \mathbf{J} and ω . In what follows, we judiciously choose $\mathbf{J}(\mathbf{r})$ and the symmetries of the unit cell to construct PhCs with a variety of intriguing spectral features (see supplemental material for details). In particular, we apply TO to design *six accidentally degenerate* modes of monopolar (M), dipolar (D) and quadrupolar (Q) profiles (inset of Fig. 1) that transform according to the A and E irreducible representations of the C_{4v} point group, and which, in turn, give rise to conical dispersions in the vicinity of their degeneracy [27, 28]. We emphasize that designing such a *six-fold* degeneracy poses a significant challenge for conventional design and even for sophisticated, heuristic optimization algorithms such as particle swarms, simulated annealing, or genetic algorithms [29–31], but can be susceptible to efficient gradient-based TO techniques, in combination with a proper problem formulation.

Figure 1 shows a topology-optimized PhC unit cell and its associated band structure, which exhibits two overlapping DCs at the Γ point, one with transverse electric (TE) and the other with transverse magnetic (TM) polarization. Note that the DC in our design is the so-called generalized DC typically characterized by the presence of an extra flat band [32]. Within the DPDC, TM Dirac bands are formed by the degeneracy of one monopolar (M) and two dipolar (D) modes, whereas TE Dirac bands are formed by the degeneracy of two dipolar (D) and one quadrupolar (Q) modes. The optimized structure consists of high dielectric regions ($\epsilon_r = 5.5$), typical of common materials such as silicon nitride or titania, in a background of air ($\epsilon_r = 1$). Intermediate permittivities, $\epsilon_r \in (1, 5.5)$, are also seen as a result of fine-tuning the necessary modal frequencies to ensure a perfect overlap. The resulting *gray-scale* PhC has altogether *six* DPDC modes whose

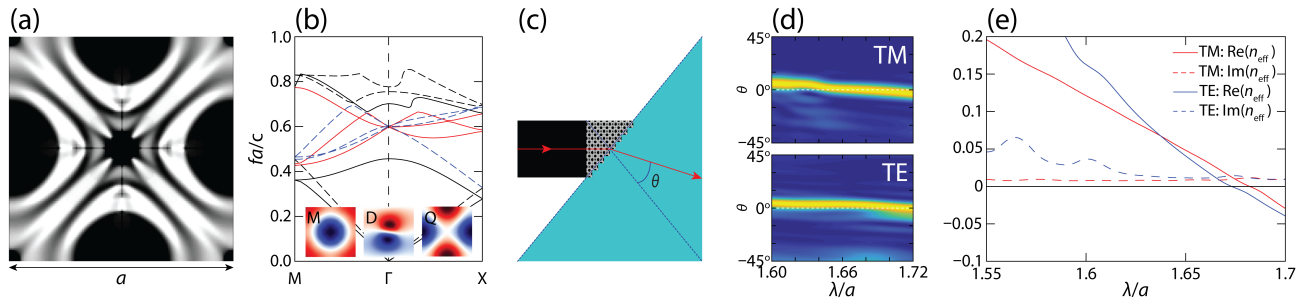


FIG. 1. (a) Topology-optimized unit cell. Black (white) regions have relative permittivity $\epsilon_r \approx 5.5$ ($\epsilon_r = 1$). Gray regions with intermediate permittivities are also seen. Note that the structure obeys C_{4v} symmetry. (b) The band structure reveals two overlapping Dirac cones, one for TM polarization (solid lines) and the other for TE polarization (dashed lines). Transverse magnetic Dirac bands (dark red lines) are formed by the degeneracy of one monopolar (M) and two dipolar (D) modes manifested by the E_z component whereas transverse electric Dirac bands (light blue lines) are formed by the degeneracy of two dipolar (D) and one quadrupolar (Q) modes manifested by the H_z component (see figure inset). (c) Configuration of the prism test designed to illustrate effective zero index behavior for designs with dual polarization Dirac cones (DPDC). (d) FDTD analysis of the DPDC structures and their farfield patterns through the prism test show orthogonally emerging beams at the prism facet ($\theta = 0$), validating the effective zero index behavior for both TM- and TE-polarized waves incident on the non-binary design. Also shown are the retrieved TM and TE effective indices for the non-binary design (e).

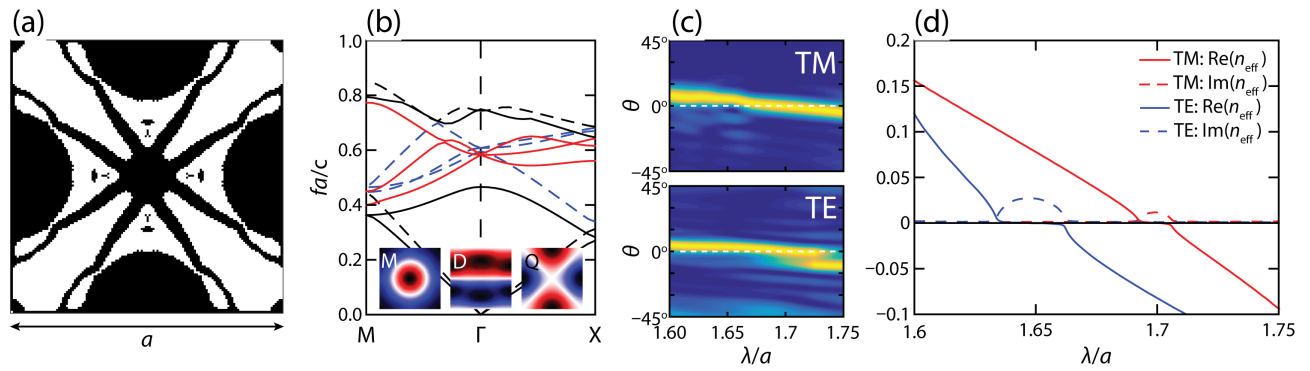


FIG. 2. (a) Binary regularized version of DPDC PhC unit cell, with the corresponding band structure (b) showing TM (solid lines) and TE (dashed lines) Dirac cones. FDTD analysis and the farfield patterns through the prism test show orthogonally emerging beams at the prism facet ($\theta = 0$), validating the effective zero index behavior for both TM- and TE-polarized incident waves. (d) Also shown are the TM and TE effective indices retrieved from scattering coefficients.

frequencies are degenerate to within 0.1%, an accuracy limited only by numerical resolution. Here, we note that in a few initial rounds of optimization, we deliberately optimize for a TM quadrupole at $f_{\text{TMQ}} \sim 0.75f_{\text{D}}$ and a TE monopole at $f_{\text{TEM}} \sim 1.25f_{\text{D}}$ in addition to the six degenerate modes forming the DC. We find that such a procedure for “mode separation” helps ensure well-isolated conical dispersions.

DCs at the center of the Brillouin zone correspond to zero-index behavior when the appropriate homogenization criteria are met [1, 3]. We perform full-wave FDTD analysis on our DPDC structures and show that they indeed exhibit various zero-index characteristics. One characteristic of a zero-index medium (ZIM) is observed in the so-called “prism” test [3], where plane waves normally incident on a facet of a zero-index prism emerge at right angle from another facet. Alternatively, one can also simulate the complex transmission and reflection coefficients of the zero-index medium, from which effective constitutive parameters can be extracted [1, 3]. As shown in Figure 1(c), we perform a prism test by illuminating

one side of a 45-45-90° triangular region made up of DPDC unit cells and then measuring the far-field patterns emerging out of the diagonal (hypotenuse) facet. Note that θ is the refraction angle between the direction of the emerging beam and the facet normal. Figure 1(d) shows smooth Gaussian beam profiles in the far field with the refraction angles crossing zero around the Dirac-cone wavelengths for both TE and TM polarizations. Index retrievals (Fig. 1e) also confirm the zero-index behavior with the effective index crossing $n = 0$ between 1.6–1.7 λ/a . It must be noted that in our structures, zero-index behavior is only observed for normal incidence; illumination at oblique incident angles excite modes which do not exhibit zero-index behavior, as is the case for most Dirac-cone zero-index media [33].

While Fig. 1 demonstrates a perfect DPDC, the grayscale dielectric profile poses a significant fabrication challenge (though it may be implemented in the radio frequency regime). Here, we examine a binary regularized version better suited for experimental realization. The modified structure

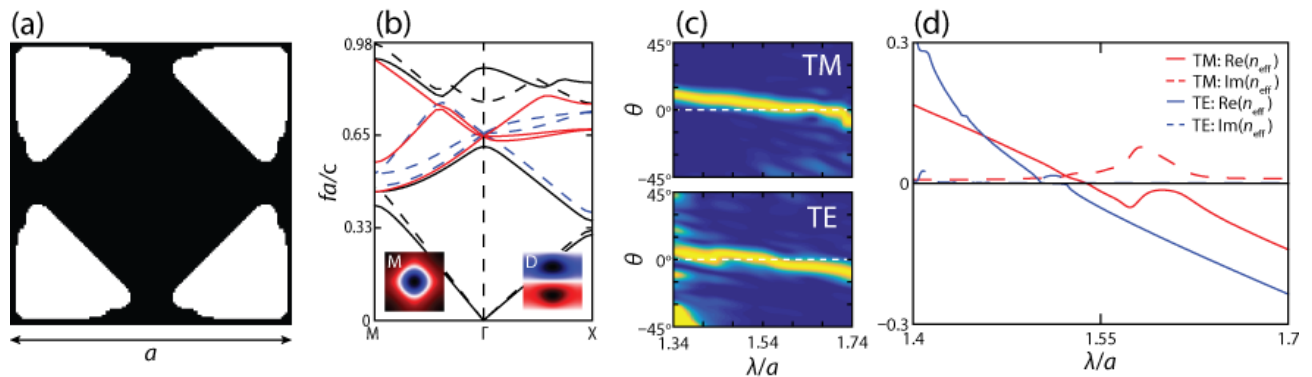


FIG. 3. (a) Binary regularized DPDC PhC with fabrication-friendly features. (b) The corresponding band structure shows two overlapping TM (solid lines) and TE (dashed lines) Dirac cones. (c) FDTD analysis and the farfield patterns through the prism test [Fig. 3(a)] show orthogonally emerging beams at the prism facet ($\theta = 0$), validating the effective zero index behavior for both TM- and TE-polarized incident waves. (d) Also shown are the TM and TE retrieved effective indices.

(Fig. 2a) is obtained via two stages: first, we apply threshold projection filters [34] *during* the optimization process to produce a binary design; then, we feed the intermediate binary design into a *post-optimization* pixel-averaging routine to weed out the fine features and regularize the structure (see also the supplemental material). The associated band structure (Fig. 2b) shows a DPDC albeit with a *spoiled* overlap due to a small frequency gap of $\sim 1\%$ between the TE and TM DCs. Figure 2(c,d) show the corresponding prism tests and index retrieval analyses. Arguably, the optimally fine-tuned gray-scale structure shows better performance than the completely binary version. This is due to following reasons: for the gray-scale version, the zero-index crossing is perfectly linear and virtually degenerate for both polarizations; for the binary version, the crossings are separated by about 1% and real part of the effective index shows a constant zero value while the imaginary part depicts a bump around the zero crossing, which corresponds to a small bandgap near the Dirac-point frequency [3]. Nevertheless, the modified structures clearly feature a range of wavelengths where *near-zero-index* behavior is observed for both polarizations, which make them realistic candidates for practical applications. We note that an approach to realize DPDCs and polarization-independent zero-index behavior was recently proposed [35], which necessitates the use of complex meta-crystals based on patterning an anisotropic elliptic metamaterial. In contrast, we identify DPDCs by virtue of unconventional geometries that can be imprinted on simple ordinary isotropic dielectrics.

The appearance of complicated features in the DPDC geometry (Fig. 1) can be attributed to numerous stringent conditions imposed upon the optimization process. As noted above, one such condition is the mode separation constraint which pushes certain extraneous modes away from the Dirac degeneracy. We find that relaxing this constraint leads to a simple DPDC structure with regular geometric features (Fig. 3a) although the proximity of an unintentional TM quadrupole mode in the band structure engenders an anti-crossing (aka mode mixing [36]) off the Γ point near the Dirac fre-

quency (Fig. 3b). Nevertheless, FDTD analyses of Fig. 3(a) clearly show the near-zero-index behavior (Fig. 3c,d) for both polarizations. Note that the simple “four-hole” structure (Fig. 3a) has a relative permittivity $\epsilon = 3.3$, making it suitable for fabrication with common polymer materials.

Dirac Cones at the K point.— To demonstrate the versatility of our approach, we proceed to design DPDCs based on a hexagonal lattice with symmetry properties distinct from those found on a square lattice. In particular, we focus on the **K** point of the Brillouin zone, where two dipolar eigenmodes that transform according to the E irreducible representations of C_{3v} point group form a *deterministic* DC, i.e., a DC that arises as a consequence of the symmetry of the lattice [27, 28]. We show that we can overlap two such DCs, one with TM polarization and the other with TE polarization, thus restoring electromagnetic duality [12] in the vicinity of the four-fold degenerate Dirac point. Specifically, we employ the LDOS TO formulation to design degenerate TM and TE dipolar modes while imposing C_{3v} symmetry via suitable transformations which ensure the concurrence of the corresponding degenerate partner for each polarization, leading to DPDCs.

Figure 4 shows complex geometries discovered by TO and the corresponding band structure with overlaid TE and TM DCs at **K** point. The gap between the two Dirac points is as small as $< 0.1\%$, only limited by numerical discretization errors. To our knowledge, this structure is the first proof-of-principle 2D design, based on ordinary isotropic dielectric materials, that hosts overlaid TE/TM DCs at a non- Γ point of a PhC. Moreover, this structure stands in contrast to more sophisticated recent designs using 2D metacrystals [12] or 3D hexagonal PhC [21]. Since DPDCs at the **K** point of a hexagonal lattice are important precursors to non-trivial topological states [11, 12, 21], our method suggests an alternative precursor from which one may realize a so-called photonic topological insulator (PTI). Since our focus here is realizing DPDCs, we will not pursue making a PTI here. However, it is worth mentioning that there are well-known techniques to introduce non-trivial topological bandgaps into DPDCs based on suit-

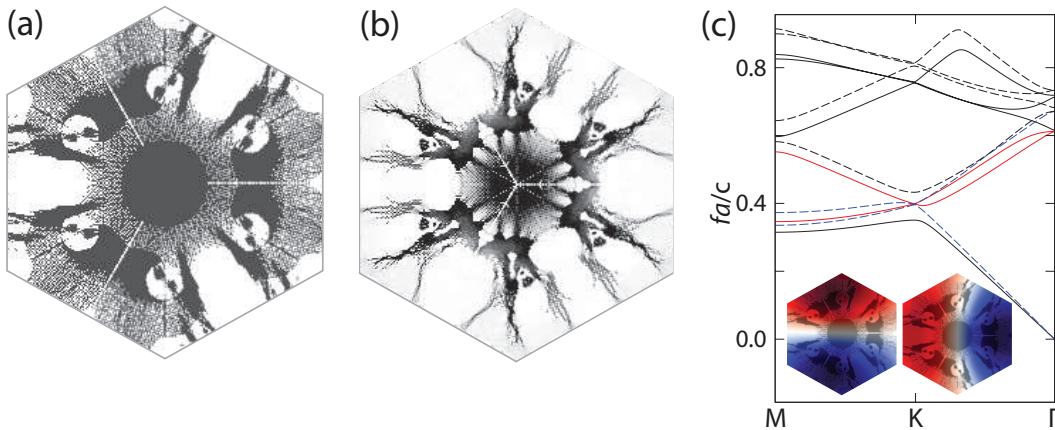


FIG. 4. Detailed image of (a) low-index ($\epsilon_r = 3.3$) (b) high-index ($\epsilon_r = 9$) topology-optimized hexagonal unit cell. (c) Band structure of the low-index design exhibiting overlaid TE (dashed line) and TM (solid lines) Dirac bands (red and blue). The degenerate modes (insets) transform according to the E irreducible representation of C_{3v} group.

able bi-anisotropic perturbations, such as by introducing off-axis propagation ($k_z \neq 0$), by systematic reduction of mirror symmetry, or by modifications that mix TE and TM polarizations while preserving the pseudospin distinction [12]. Although the TO-discovered geometry might be quite challenging to fabricate due to the existence of pixel-thin hairy features, we note that these features do not indicate a fundamental limitation of our technique but are an artifact of underlying image-transformation steps which impose undue constraints on the optimization process. In the supplement, we discuss such drawbacks as well as possible ways to mitigate them.

Conclusion and remarks.— While some of the optimized designs we have presented might prove challenging, though not impossible, to fabricate at visible or near-infrared frequencies, they can be readily realized at mid- to far-IR as well as microwave frequencies via existing technologies such as computerized machining, 3D printing, laser cutting, additive manufacturing, or two-photon lithography, self-assembly of DNA molecules [37–40]. Furthermore, thin isolated features which typically beset topology-optimized designs can be removed by a variety of advanced regularization and averaging techniques [15]. The appearance of such features indicates an optimization process that is severely constrained by the design requirements of realizing TE and TM modes with the same modal profile at the same frequency. The fundamental issue underlying such a design is that in a generic structured isotropic 2D medium, TM bands tend to be at lower frequencies than TE bands, breaking the so-called electromagnetic duality. While we have shown that our TO formulation is capable of restoring this duality and finding DPDCs on a 2D lattice, this comes at the expense of a highly irregular structure which needs to be fine-tuned with thin sensitive features. In contrast, we surmise that three-dimensional platforms will offer even greater flexibility. For example, it is known that TM modes tend to experience effectively different index of refraction relative to TE modes in 3D PhC slabs, e.g. depending on

whether the PhC geometry consists of holes or pillars [36]. In future work, we will consider optimization in full 3D multi-layered geometries, which we expect will open up even more exciting opportunities for new structural designs in the fields of metasurfaces, metamaterials and topological photonics.

Acknowledgements.— The authors thank Philip Camayd-Muñoz and Orad Reshef for discussions. This work was partially supported by the Air Force Office of Scientific Research under Contract No. FA9550-14-1-0389, by the National Science Foundation under Grants No. DMR-1454836 and DMR-1360889, and by the Princeton Center for Complex Materials, a MRSEC supported by NSF Grant No. DMR-1420541. Z. Lin is supported by the National Science Foundation Graduate Research Fellowship Program under Grant No. DGE1144152.

* These authors contributed equally to this work.

† loncar@seas.harvard.edu

- [1] Xueqin Huang, Yun Lai, Zhi Hong Hang, Huihuo Zheng, and C. T. Chan. Dirac cones induced by accidental degeneracy in photonic crystals and zero-refractive-index materials. *Nature Materials*, 10(8):582–586, Aug 2011.
- [2] Parikshit Moitra, Yuanmu Yang, Zachary Anderson, Ivan I Kravchenko, Dayrl P Briggs, and Jason Valentine. Realization of an all-dielectric zero-index optical metamaterial. *Nature Photonics*, 7(10):791–795, 2013.
- [3] Yang Li, Shota Kita, Philip Camayd-Muñoz, Orad Reshef, Daryl I Vulis, Mei Yin, Marko Lončar, and Eric Mazur. On-chip zero-index metamaterials. *Nature Photonics*, 9(11):738–742, 2015.
- [4] Hodjat Hajian, Ekmel Ozbay, and Humeyra Caglayan. Realization of zero-refractive-index lens with ultralow spherical aberration. *Applied Physics Letters*, 109:031105, July 2016.
- [5] Xin-Tao He, Zhi-Zhen Huang, Ming-Li Chang, Shao-Zeng Xu, Fu-Li Zhao, Shao-Zhi Deng, Jun-Cong She, and Jian-Wen Dong. Realization of zero-refractive-index lens with ultralow spherical aberration. *ACS Photonics*, 3:2262–2267, December

- 2016.
- [6] Inigo Liberal and Nader Engheta. Near-zero refractive index photonics. *Nature Photonics*, 11:149–158, March 2017.
- [7] Shota Kita, Yang Li, Philip Camayd-Muñoz, Orad Reshef, Daryl I. Vulis, Robert W. Day, Eric Mazur, and Marko Lončar. On-chip all-dielectric fabrication-tolerant zero-index metamaterials. *Optics Express*, 25(7):8326–8334, 2017.
- [8] B. Zhen, C. W. Hsu, Y. Igarashi, L. Lu, I. Kaminer, A. Pick, S-L Chua, J. D. Joannopoulos, and M. Soljačić. Spawning rings of exceptional points out of dirac cones. *Nature*, 525:354–358, 2015.
- [9] Zin Lin, Adi Pick, Marko Lončar, and Alejandro W Rodriguez. Enhanced spontaneous emission at third-order dirac exceptional points in inverse-designed photonic crystals. *Physical Review Letters*, 117(10):107402, 2016.
- [10] Xiangdong Zhang. Observing zitterbewegung for photons near the dirac point of a two-dimensional photonic crystal. *Physical review letters*, 100(11):113903, 2008.
- [11] Ling Lu, John D Joannopoulos, and Marin Soljačić. Topological photonics. *Nature Photonics*, 8(11):821–829, 2014.
- [12] Alexander B Khanikaev, S Hossein Mousavi, Wang-Kong Tse, Mehdi Kargarian, Allan H MacDonald, and Gennady Shvets. Photonic topological insulators. *Nature materials*, 12(3):233–239, 2013.
- [13] Daryl I Vulis, Yang Li, Orad Reshef, Philip Camayd-Muñoz, Mei Yin, Shota Kita, Marko Lončar, and Eric Mazur. Monolithic cmos-compatible zero-index metamaterials. *arXiv preprint arXiv:1610.05368*, 2016.
- [14] Ole Sigmund and Jakob Søndergaard Jensen. Systematic design of phononic band-gap materials and structures by topology optimization. *Philosophical Transactions of the Royal Society of London A: Mathematical, Physical and Engineering Sciences*, 361(1806):1001–1019, 2003.
- [15] J.S. Jensen and O. Sigmund. Topology optimization for nanophotonics. *Laser and Photonics Reviews*, 5(2):308–321, 2011.
- [16] Xiangdong Liang and Steven G Johnson. Formulation for scalable optimization of microcavities via the frequency-averaged local density of states. *Optics express*, 21(25):30812–30841, 2013.
- [17] Alexander Y Piggott, Jesse Lu, Konstantinos G Lagoudakis, Jan Petykiewicz, Thomas M Babinec, and Jelena Vučković. Inverse design and demonstration of a compact and broadband on-chip wavelength demultiplexer. *Nature Photonics*, 9(6):374–377, 2015.
- [18] Jesse Lu and Jelena Vučković. Nanophotonic computational design. *Optics express*, 21(11):13351–13367, 2013.
- [19] Bing Shen, Peng Wang, Randy Polson, and Rajesh Menon. An integrated-nanophotonics polarization beamsplitter with $2.4 \times 2.4 \mu\text{m}^2$ footprint. *Nature Photonics*, 9(6):378–382, 2015.
- [20] Zin Lin, Xiangdong Liang, Marko Lončar, Steven G Johnson, and Alejandro W Rodriguez. Cavity-enhanced second-harmonic generation via nonlinear-overlap optimization. *Optica*, 3(3):233–238, 2016.
- [21] A Slobozhanyuk, SH Mousavi, X. Ni, D. Smirnova, Y Kivshar, and A.B. Khanikaev. Three-dimensional all-dielectric photonic topological insulator. *arXiv preprint arXiv:1602.00049*, 2016.
- [22] Qiming Wang, Julie A Jackson, Qi Ge, Jonathan B Hopkins, Christopher M Spadaccini, and Nicholas X Fang. Lightweight mechanical metamaterials with tunable negative thermal expansion. *Physical review letters*, 117(17):175901, 2016.
- [23] AP Drozdov, MI Eremets, IA Troyan, V Ksenofontov, and SI Shylin. Conventional superconductivity at 203 kelvin at high pressures in the sulfur hydride system. *Nature*, 525(7567):73–76, 2015.
- [24] Zhao Qin, Gang Seob Jung, Min Jeong Kang, and Markus J Buehler. The mechanics and design of a lightweight three-dimensional graphene assembly. *Science Advances*, 3(1):e1601536, 2017.
- [25] Zi Jing Wong, Ye-Long Xu, Jeongmin Kim, Kevin O’Brien, Yuan Wang, Liang Feng, and Xiang Zhang. Lasing and anti-lasing in a single cavity. *Nature Photonics*, 10(12):796–801, 2016.
- [26] Xiangdong Liang and Steven G. Johnson. Formulation for scalable optimization of microcavities via the frequency-averaged local density of states. *Opt. Express*, 21(25):30812–30841, Dec 2013.
- [27] Kazuaki Sakoda. Proof of the universality of mode symmetries in creating photonic dirac cones. *Opt. Express*, 20(22):25181–25194, 2012.
- [28] Jun Mei, Ying Wu, Che Ting Chan, and Zhao-Qing Zhang. First-principles study of dirac and dirac-like cones in phononic and photonic crystals. *Physical Review B*, 86(3):035141, 2012.
- [29] Scott Kirkpatrick. Optimization by simulated annealing: Quantitative studies. *Journal of statistical physics*, 34(5):975–986, 1984.
- [30] David E Goldberg and John H Holland. Genetic algorithms and machine learning. *Machine learning*, 3(2):95–99, 1988.
- [31] James Kennedy. Particle swarm optimization. In *Encyclopedia of machine learning*, pages 760–766. Springer, 2011.
- [32] Balázs Dóra, Janik Kailasvuori, and R. Moessner. Lattice generalization of the dirac equation to general spin and the role of the flat band. *Phys. Rev. B*, 84:195422, Nov 2011.
- [33] Peng Zhang, Chris Fietz, Philippe Tassin, Thomas Koschny, and Costas M Soukoulis. Numerical investigation of the flat band Bloch modes in a 2d photonic crystal with dirac cones. *Optics express*, 23(8):10444–10452, 2015.
- [34] Fengwen Wang, Boyan Stefanov Lazarov, and Ole Sigmund. On projection methods, convergence and robust formulations in topology optimization. *Structural and Multidisciplinary Optimization*, 43(6):767–784, 2011.
- [35] Jia-Rong Wang, Xiao-Dong Chen, Fu-Li Zhao, and Jian-Wen Dong. Full polarization conical dispersion and zero-refractive-index in two-dimensional photonic hypercrystals. *Scientific reports*, 6, 2016.
- [36] J. D. Joannopoulos, S. G. Johnson, J. N. Winn, and R. D. Meade. *Photonic crystals: molding the flow of light*. Princeton university press, 2011.
- [37] R.A. Borisov, G.N. Dorojkina, N.I. Koroteev, V.M. Kozenkov, S.A. Magnitskii, D.V. Malakhov, A.V. Tarasishin, and A.M. Zheltikov. Fabrication of three-dimensional periodic microstructures by means of two-photon polymerization. *Applied Physics B*, 67(6):765–767, 1998.
- [38] Anders Clausen, Fengwen Wang, Jakob S. Jensen, Ole Sigmund, and Jennifer A. Lewis. Topology optimized architectures with programmable poisson’s ratio over large deformations. *Advanced Materials*, 27(37):5523–5527, 2015.
- [39] Caroline Pouya, Johannes T. B. Overvelde, Mathias Kolle, Joanna Aizenberg, Katia Bertoldi, James C. Weaver, and Pete Vukusic. Characterization of a mechanically tunable gyroid photonic crystal inspired by the butterfly parides sesostris. *Advanced Optical Materials*, 4(1):99–105, 2016.
- [40] Paul W. K. Rothmund. Folding dna to create nanoscale shapes and patterns. *Nature*, 440:297–302, March 2006.